lubricants

MDPI

Article

Graphite Fluoride as a Novel Solider Lubricant Additive for Ultra-High-Molecular-Weight Polyethylene Composites with Excellent Tribological Properties

Guodong Huang [1,*], Tao Zhang [1], Yi Chen [1], Fei Yang [1], Huadong Huang [2] and Yongwu Zhao [3]

[1] School of Mechanical Technology, Wuxi Institute of Technology, Wuxi 214121, China; zhangt@wxit.edu.cn (T.Z.)
[2] Department of Precision Manufacturing Engineering, Suzhou Institute of Industrial Technology, Suzhou 215104, China
[3] School of Mechanical Engineering, Jiangnan University, Wuxi 214122, China
* Correspondence: huanggd@wxit.edu.cn

Abstract: The tribological properties of ultra-high-molecular-weight polyethylene (UHMW-PE) play a significant role in artificial joint materials. Graphite fluoride (GrF), a novel solid lubricant, was incorporated into ultra-high-molecular-weight polyethylene (UHMW-PE) at different concentrations via ball milling and heat pressing to prepare the GrF-UHMW-PE composites. The structure, hardness, and tribological behavior of the composites were investigated using X-ray diffraction (XRD), Fourier-transform infrared (FT-IR) spectrometry, ball indentation hardness, and a reciprocating ball-on-plane friction tester, respectively. The results of FT-IR showed that hydrogen bonds (C-F···H-C) could be formed between GrF and UHMW-PE. The hardness of the composites was significantly enhanced by increasing the GrF concentrations. GrF in the composites displayed superior lubricant properties and the coefficient of friction (COF) of the composites was significantly decreased at lower concentrations of GrF viz. 0.1 and 0.5 wt%. The addition of GrF also significantly enhanced the anti-wear properties of the composites, which was a combined effect of lubrication as well as hardness provided by GrF. At 0.5 wt% GrF concentration, the COF and the wear rate were reduced by 34.76% and 47.72%, respectively, when compared to UHMW-PE. As the concentration of GrF increased, the wear modes of the composites transitioned from fatigue wear to abrasive wear. Our current work suggested that GrF-UHMW-PE composites could be a suitable candidate for artificial joint materials.

Keywords: polymer composites; ultra-high-molecular-weight polyethylene (UHMW-PE); graphite fluoride (GrF); hardness; wear mechanism

Citation: Huang, G.; Zhang, T.; Chen, Y.; Yang, F.; Huang, H.; Zhao, Y. Graphite Fluoride as a Novel Solider Lubricant Additive for Ultra-High-Molecular-Weight Polyethylene Composites with Excellent Tribological Properties. *Lubricants* **2023**, *11*, 403. https://doi.org/10.3390/lubricants11090403

Received: 25 August 2023
Revised: 12 September 2023
Accepted: 13 September 2023
Published: 15 September 2023

1. Introduction

Ultra-high-molecular-weight polyethylene (UHMW-PE) is considered a unique engineering plastic with excellent performance [1]. Owing to its chemical inertness [2], low friction coefficient [3], wear resistance [4], and good biocompatibility [5], UHMW-PE has already been applied as a bearing surface for total hip replacements since the 1960s [6] and is currently regarded as the gold standard material [7] used in this domain. However, due to the prolonged use of hip prostheses, wear debris of UHMW-PE is generated and can induce periprosthetic osteolysis [8], which may eventually lead to the failure of the total hip arthroplasty. This causes patient suffering and increased financial burden. In order to improve the longevity of total hip and alleviate the patient's pain, it is important to improve the anti-wear properties of UHMW-PE materials. Therefore, researchers have developed numerous approaches [7,9,10] to enhance the wear resistance of UHMW-PE, and one effective method has been the incorporation of reinforcing fillers.

Carbon-based materials, such as graphite [11], graphene nanoplatelets (GNPs) [12,13], graphene oxide (GO) [14], carbon nanotubes (CNTs) [15], and carbon fiber (CFs) [16], have

not only exceptional mechanical and tribological properties, but also excellent biocompatibility, which have been utilized in reinforcing fillers for polymers. Currently, much study has already been conducted on this subject. Adding GO to UHMW-PE can significantly improve the hardness [17],yield strength [18], and anti-wear resistance [19]. UHMW-PE-filled CNTs [7] can efficiently enhance the tribological properties of UHMW-PE. As a superior reinforcement material for UHMW-PE, graphene can improve the tensile and creep-resistance properties of UHMW-PE [20]. And graphene-UHMW-PE composites have also shown higher hardness and lower friction [21] than pure UHMW-PE. Furthermore, Reddy K.S.N. et al. [22] also pointed out that UHMW-PE-filled graphite could significantly improve its tribological behavior. According to the aforementioned research findings, it can be inferred that UHMW-PE-filled carbon materials have the potential to extend the service life of artificial joints.

Graphite fluoride (GrF) is an important derivative of graphite with the molecular formula (CFx)n ($0 < x < 1.25$), which is obtained by the direct reaction of graphite with fluoride gas at a controlled pressure and temperature. During the chemical reaction process, fluorine atoms bind with carbon atoms to form covalent C-F bonds, which result in the conversion of some C-C bonds from sp2 to sp3 hybridization [23]. The presence of F atoms in graphite endows GrF with unique lubrication properties, excellent chemical stability, extremely low surface energy, outstanding thermal conductivity, and stability. As a result, GrF has gained substantial attention in recent years, and it has already been employed in a variety of disciplines such as solar cells [24], batteries [25], sensors [26], supercapacitors [27], hydrophobic coatings [28], and lubricants [29]. Among the various applications, GrF, a well-known solid lubricant, has gained increasing attention. In comparison to graphite and molybdenum disulfide (MoS2), GrF has demonstrated a superior lubrication performance relative to conventional solid lubricants due to its expanded interlamellar space [30] and its low surface energy [31]. Burnished GrF on stainless-steel disks showed lower friction coefficients than MoS2 and graphite, and the wear lives of GrF film were also longer than them at 400 °C [32]. At high temperature, polyimide-bonded GrF [33] showed a lower friction and longer lifetime than polyimide-bonded MoS2. Comparing and analyzing the tribological properties of polytetrafluoroethylene (PTFE)-GrF and PTFE-MoS_2 composites, Yan et al. [34] found that GrF could considerably reduce the friction coefficient and enhance the anti-wear performance of PTFE in comparison to MoS2. These experiments focused primarily on the lubricant properties of GrF at a high temperature. However, the lubricative property of GrF in polymer composites has been little-reported at room temperature, and the anti-wear mechanism of GrF-polymer composites is ambiguous. In addition, the effect of GrF addition content on their tribological properties remains unclear.

According to our knowledge, there have been few reports on GrF-UHMW-PE composites. In this study, GrF is used as the solid lubricant additive and incorporated into a matrix of UHMW-PE. GrF-UHMW-PE composites are prepared. The effect of the GrF content on the mechanical and tribological properties of a UHMW-PE matrix was systematically investigated.

2. Materials and Methods

2.1. Materials

The Commercial UHMW-PE (GRU1050) powder was offered by Ticona/Celanese (Dallas, TX, USA). GrF powder with a 52–60 wt% fluoride content was purchased from Nanjing XFNANO Materials Technology Co., Ltd. (Nanjing, China). Other experimental reagents were analytically pure.

2.2. Preparation of GrF-UHMW-PE Composites

The percentage of GrF added plays an important role in the properties of the polymer. Sun et al. [35] reported that the incorporation of 0.5 wt% GrF into polyamide 6 made an optimal enhancement to its tensile strength and elastic modulus. Moreover, they [36] added 0.5 wt% and 1.0 wt% of GrF to polyamide 66 and observed a significant improvement in its tribological properties. In accordance with the aforementioned literature, the current study

involved the incorporation of GrF at varying percentages: 0 wt%, 0.1 wt%, 0.5 wt%, and 1.0 wt%.

GrF-UHMW-PE composites were prepared as follows. Various amounts, i.e., 0 wt%, 0.1 wt%, 0.5 wt%, 1.0 wt% of GrF, were mixed with the UHMW-PE powder. The powder mixture was firstly mixed evenly using mechanical ball milling, which was operated for 5 h at a rotation speed of 400 rpm at room temperature. Then, the uniformly dispersed mixture was placed into a prefabricated metal mold and cold-pressed under 5 MPa for 15 min at room temperature. Immediately after, the mixture was transferred into a hot-air oven and heated for 2 h at 200 °C. After the heating process, the sample was taken out into air and pressed at 10 MPa until it cooled down to room temperature. According to the process described above, GrF-UHMW-PE composites were finally obtained, and are shown in Figure 1.

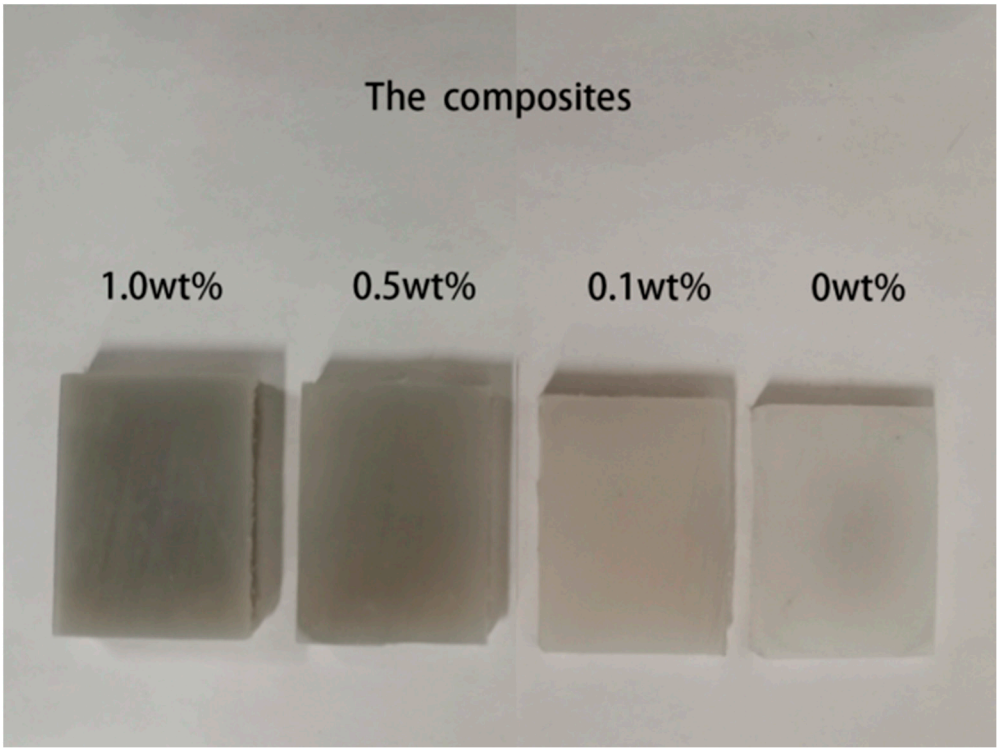

Figure 1. Photograph of GrF-UHMW-PE composites.

2.3. X-ray Diffraction (XRD) and Fourier-Transform Infrared Spectroscopy (FT-IR)

The XRD data of the samples were recorded with a Bruker D8 diffraction using a Cu K-alpha radiation. The FT-IR data of the samples were measured in Attenuated Total Reflectance (ATR) mode, by using an Alpha FT-IR spectrometer (Bruker Corporation, Ettlingen, Germany). The spectra were recorded at room temperature in a wave number range of 4000–600 cm^{-1}.

2.4. Ball Indentation Hardness

The ball indentation hardness (H) of the composites was determined based on the ISO 2039-73 standard [37]. The hardness values were measured as follows. In this experiment, a Si_3N_4 ball with a diameter of 5 mm was used as the indenter. At the beginning of testing, an initial preload of 9.8 N was carried out for 30 s. Immediately after, the sample was loaded to a peak force of 132 N and the force remained constant for 30 s. Finally, the sample was unloaded. The hardness (H) for each sample was calculated according to Equation (1):

$$H = \frac{\mathrm{P} \propto}{\mathrm{h_r} \pi \mathrm{D}(\mathrm{h} - \mathrm{h_0})};\ h_0 = h_r - \alpha \quad (1)$$

where P was the test load in N/mm, h was the maximum indentation depth in mm, D (=5) was the ball diameter in mm, α (=0.21) was a constant and h_r (=0.25) was the reduced depth of impression. Each sample's hardness test was repeated five times and the final mean value obtained from the five test results was calculated.

2.5. Tribological Testing

The contact model for the friction process is shown in Figure 2. When external force (F_n) was applied to the Si_3N_4 ceramic ball, the force and the average pressure ($\overline{p}$) between the sample and the Si_3N_4 ball could be calculated based on Hertz contact theory [38]. The calculated equations were as follows:

$$r = \sqrt[3]{\frac{3 \cdot F_n \cdot R}{4 \cdot E^*}} \tag{2}$$

$$\frac{1}{E^*} = \frac{1 - v_1^2}{E_1} + \frac{1 - v_2^2}{E_2} \tag{3}$$

$$\frac{1}{R} = \frac{1}{R_1} + \frac{1}{R_2} \tag{4}$$

$$\overline{P} = \frac{F}{\pi \cdot r^2} \tag{5}$$

where $\overline{p}$ was the average pressure in MPa, r was the contact radius in mm, F_n was the external force in N, E^* was the Effective Young's modulus in GPa, E_1 = (1 GPa) was Young's modulus of UHMW-PE in GPa, E_2 = (300 GPa) was Young's modulus of the Si_3N_4 ball in GPa, R_1 (=4.75) was the radius of the Si_3N_4 ball in mm, R_2 (=+∞) was the radius of the sample in mm, v_1 (=0.24) was Poisson's ratio of the Si_3N_4 ball and v_1 (=0.46) was Poisson's ratio of UHMW-PE. According to the research of Radovan et al. [39], the maximum contact pressure range between the ceramic ball and UHMW-PE in artificial joints during human rapid motion is 45.1 to 58.2 MPa. Therefore, based on the aforementioned equation, the predicted normal force applied was 30 N during tribological testing.

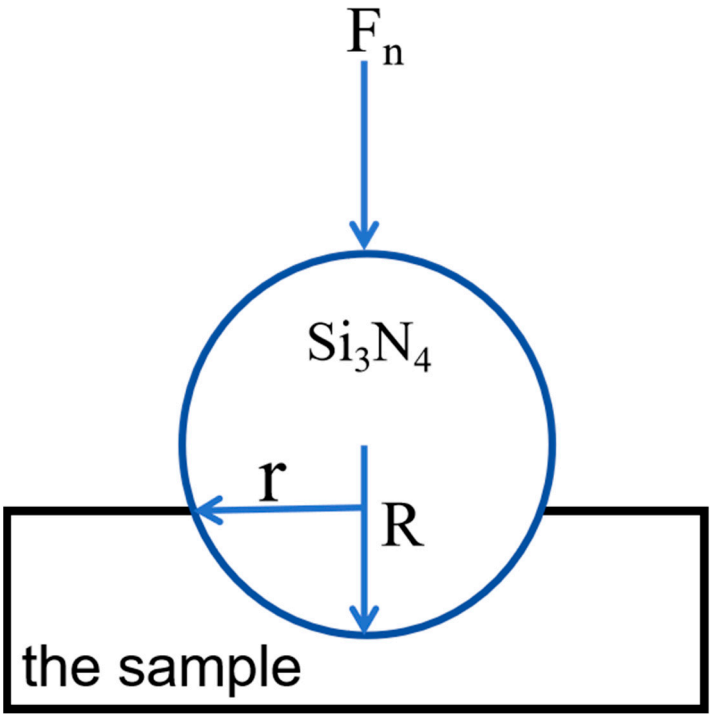

Figure 2. The contact model.

The friction and wear tests were performed on an Rtec MFT-5000 multi-function tribometer (Rtec Instruments, San Jose, CA, USA) in a linear reciprocating ball-on-flat mode. Figure 3 shows a schematic diagram of reciprocating testing. A Si_3N_4 ceramic ball with a diameter of 9.5 mm was used as the composite block counterpart. The tribological test parameters were as shown below: normal load (F_n) of 30 N, sliding frequency of 1 Hz [40], stroke length of 13 mm, and test time of 60 min [40]. During the tribological process, friction force (F_f) was recorded automatically by the MFT-500 tribometer, and the coefficient of friction (COF) was calculated simultaneously according to Equation (6):

$$\mu = \frac{F_f}{F_n} \tag{6}$$

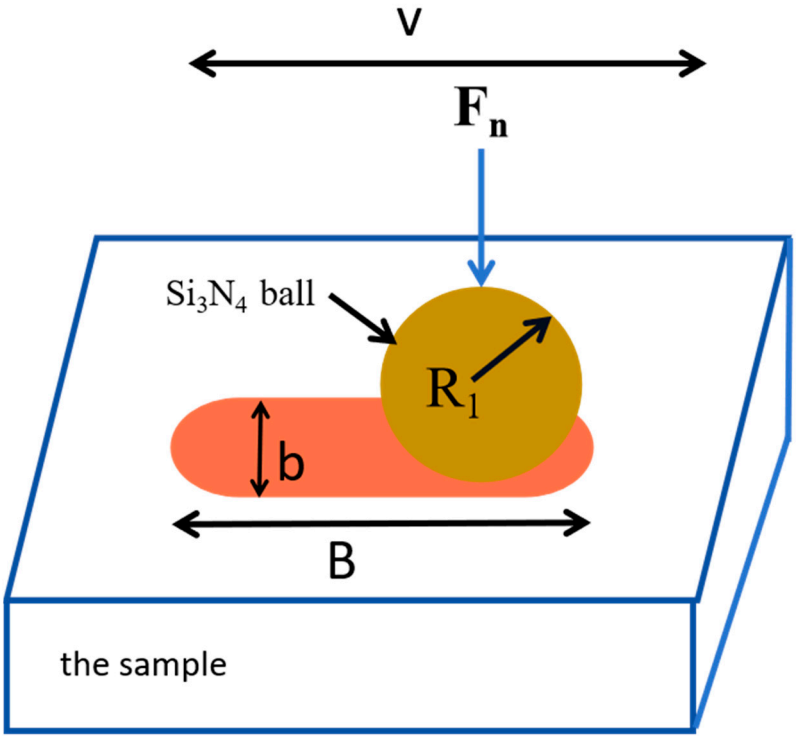

Figure 3. Schematic diagram of reciprocating testing.

After tribological tests, the wear volume (V) loss was calculated using Equation (7):

$$\mathrm{V} = \mathrm{B}\left[\frac{\pi {R_1}^2}{180}\arcsin\left(\frac{b}{2R_1}\right) - \frac{b}{2}\sqrt{{R_1}^2 - \frac{b^2}{4}}\right] \tag{7}$$

where B, b, and R_1 indicated the wear length, wear width, and the radius of a Si_3N_4 ball, respectively. The 3D and 2D profiles of the wear track were obtained using an UP-3000 3D Optical Profilometer (Rtec Instruments, USA). B and b can be calculated according to these profiles. The average wear rate (K_0) was calculated according to the following Equation (8):

$$K_0 = \frac{\mathrm{V}}{F_n \times \mathrm{L}} \tag{8}$$

where L represented the total sliding distance.

2.6. Scanning Electron Microscope (SEM)

The surface morphology of the tensile cross-section and worn surface was observed using a Scanning Electron Microscope (SEM, ZEISS Sigma HD, Oberkochen, Germany).

The samples were placed a disc, sprayed with gold and then transferred to the SEM sample platform.

3. Results and Discussion

3.1. SEM of Tensile Sections

In order to investigate the dispersion of GrF in the composites, the surface morphology of tensile cross sections was observed using SEM, as depicted in Figure 4. According to Figure 4, it found that GrF had good dispersion. It was noted that when GrF was a high filler (1.0 wt%), GrF particles were near together and might have formed the aggregation.

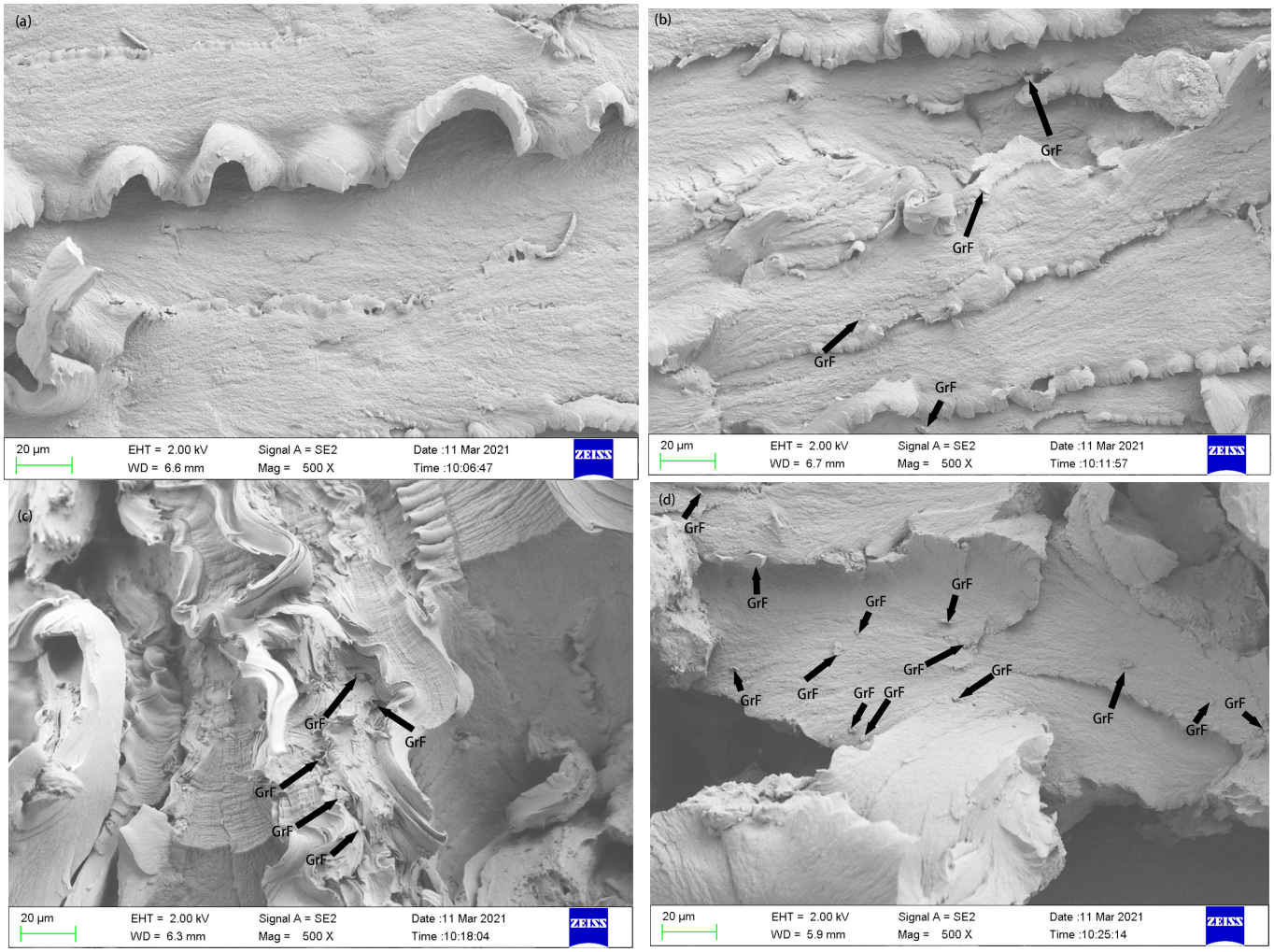

Figure 4. SEM of tensile sections: (**a**) Pure UHMW-PE, (**b**) filled 0.1 wt% GrF, (**c**) filled 0.5 wt% GrF, and (**d**) filled 1.0 wt% GrF.

3.2. XRD Patterns of the Composites

XRD is a powerful tool that we used to investigate the phase structure of materials and the dispersion of the filler in the polymer matrix. Figure 5 displays the XRD patterns of GrF and polymer composites. The laminated structure of GrF showed two characteristic diffraction peaks at 2θ = ~12.85° and ~40.70°, which were assigned to the (001) and (100) reflections, respectively. The strongest (001) diffraction peak indicated a hexagonal system compound with a much higher fluorine content. Furthermore, a broad (002) diffraction peak suggests that GrF exhibited poor ordering along the stacking direction. Moreover, a very weak peak appeared at 2θ = ~27.46°, indicating the presence of non-fluorinated graphite. Figure 5 also demonstrates that the main XRD peaks of UHMW-PE were located

at 2θ = ~21.39°, 24.05°, and 36.20°, which correspond to the (110), (200) and (020) crystal planes of UHMW-PE, respectively. According to XRD peak analysis, it was observed that the addition of GrF to UHMW-PE showed no noticeable change, suggesting that GrF was uniformly dispersed in the UHMW-PE matrix and a partially intercalated and exfoliated structure was formed in the composites. Similar XRD results were also reported for GO-UHMW-PE [41], graphene-UHMW-PE [42], and CNTs-UHMW-PE [43].

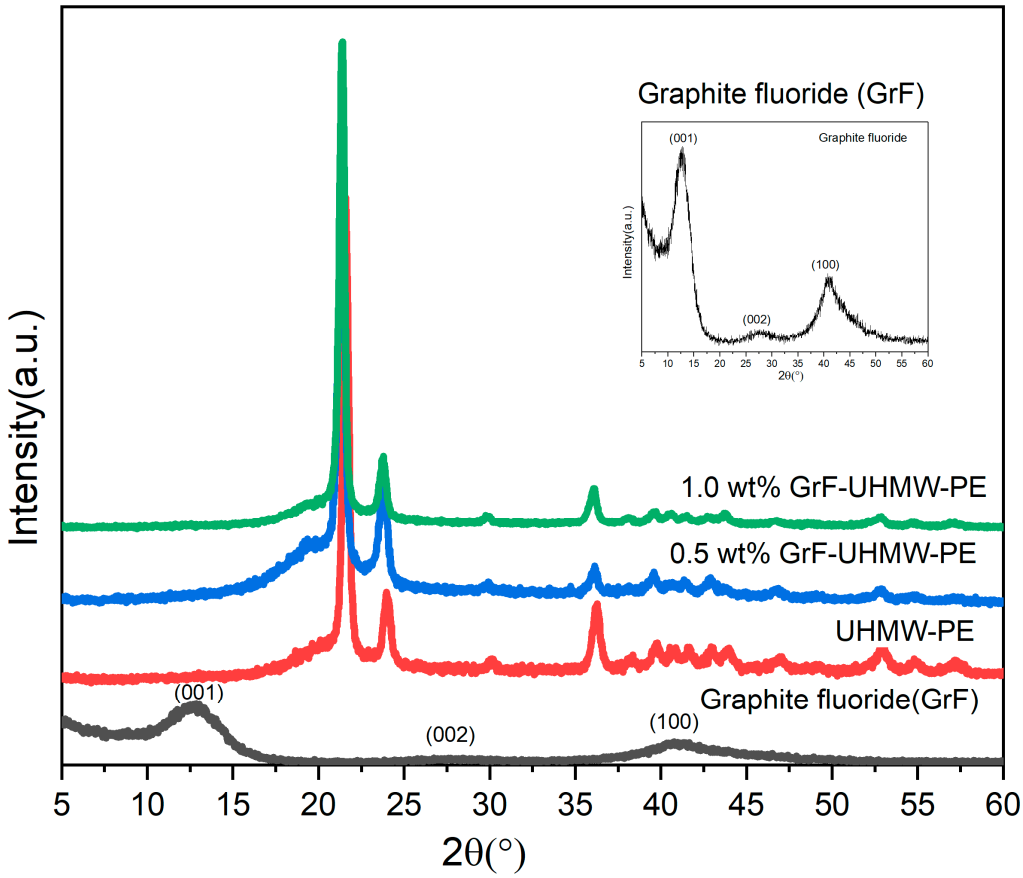

Figure 5. The XRD patterns of GrF powder and the composites.

3.3. FT-IR Spectrometry of the Composites

Figure 6 depicts the results of the FT-IR analysis of GrF and the composites, which aimed to investigate the impact of GrF on the structure of UHMW-PE. GrF exhibited two characteristic FT-IR peaks. The strongest peak at 1206 cm^{-1} was attributed to the F-C stretching vibration, while the overlapping peak at 1322 cm^{-1} represented the vibration of $–CF_2$ groups. Pure UHMW-PE has four main peaks at 720 cm^{-1}, 1462 cm^{-1}, 2840 cm^{-1}, and 2918 cm^{-1}, assigned to $–CH_2$ rock, C-H bending, C-H stretching and C-H stretching, respectively. However, when GrF (1.0 wt.%) was added to UHMW-PE, two new peaks at 1205 cm^{-1} and 1217 cm^{-1} emerged in the FT-IR spectrometry of UHMW-PE. The signal at 1205 cm^{-1} was obviously the typical absorption peak of GrF, showing that GrF was uniformly dispersed in the UHMW-PE matrix.

The emergence of a new peak at 1217 cm^{-1} in close proximity to 1205 cm^{-1} may be attributed to the formation of hydrogen bonds between GrF platelets and UHMW-PE molecular chains. A proposed mechanism for the formation of hydrogen bonds is illustrated in Figure 7. During the manufacturing process, F atoms on the GrF platelets could react with H atoms on UHMW-PE molecules to form C-F···H-C hydrogen bonds, which resulted in a new peak at 1217 cm^{-1} appearing. Similar experimental results have also been observed in GrF-PV6 composites [35]. The interaction between GrF and PV6 led to the formation of the hydrogen bonds, which contributed to the good adhesion and

dispersion of GrF in the PV6 matrix. In addition, Thalladi et al. [44] noted that certain fluorinated compounds contained hydrogen bonds that could impact the properties of the compound. Thus, it was suggested that hydrogen bonding in the GrF-UHMW-PE composites could enhance the interaction between the fillers and the matrix and improve their mechanical and tribological properties.

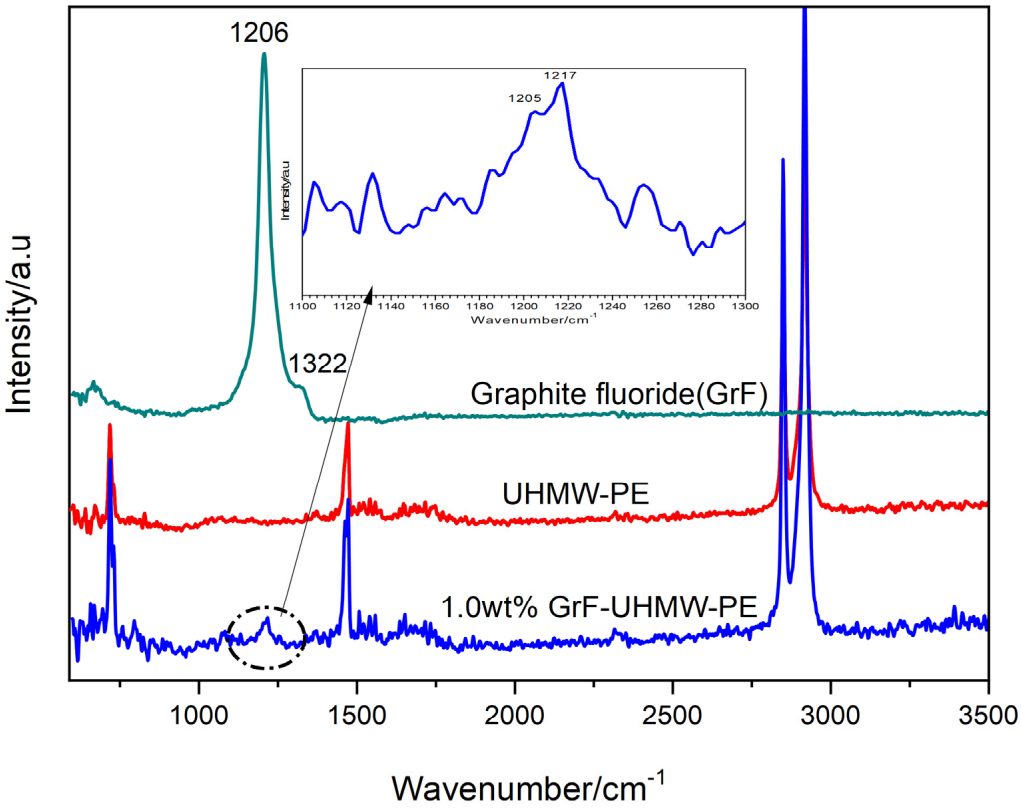

Figure 6. FT-IR spectrometry of GrF powder and the composites.

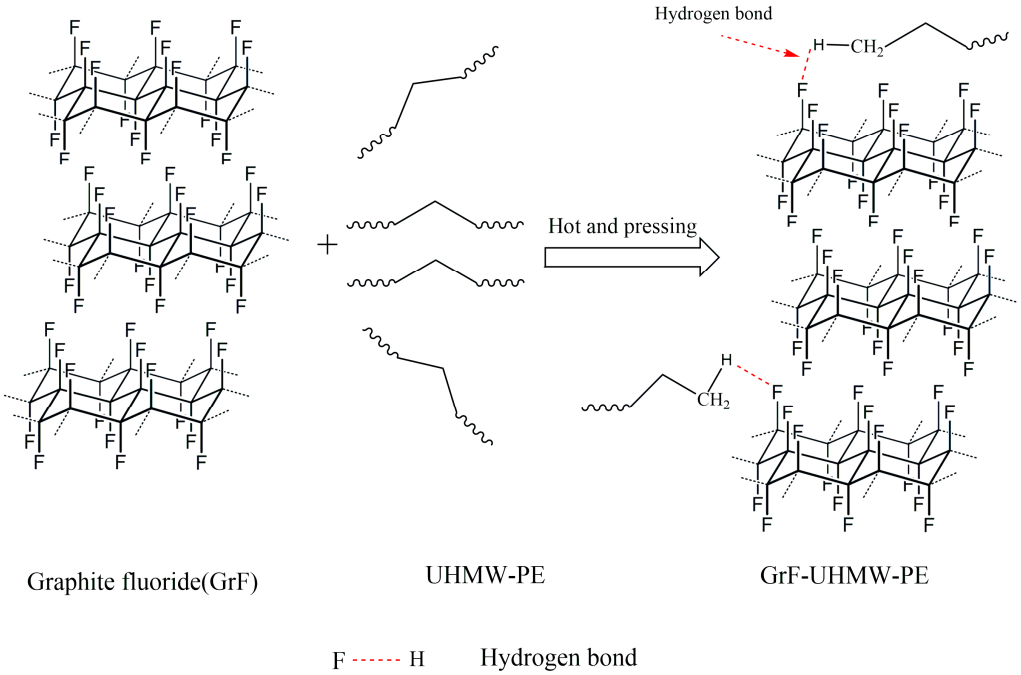

Figure 7. Proposed hydrogen bond formation mechanism.

3.4. The Hardness of the Composites

In order to investigate the effect of GrF filler on the mechanical properties of the UHMW-PE matrix, the experimental results of hardness are shown in Figure 8. As can be noted, the hardness of the GrF-UHMW-PE composites gradually increased with increasing GrF filler concentrations. The incorporation of 0.1 wt% GrF significantly increased the hardness of pure UHMW-PE and the hardness increased from an initial value of 23.97 MPa to 29.77 MPa, an increment of 24%. With the further addition of GrF to a concentration of 1.0 wt%, the hardness showed a significant increase to 32.95 MPa with an increment of 37%. These experimental results indicated that adding a lower amount of GrF could remarkably enhance the hardness of UHMW-PE.

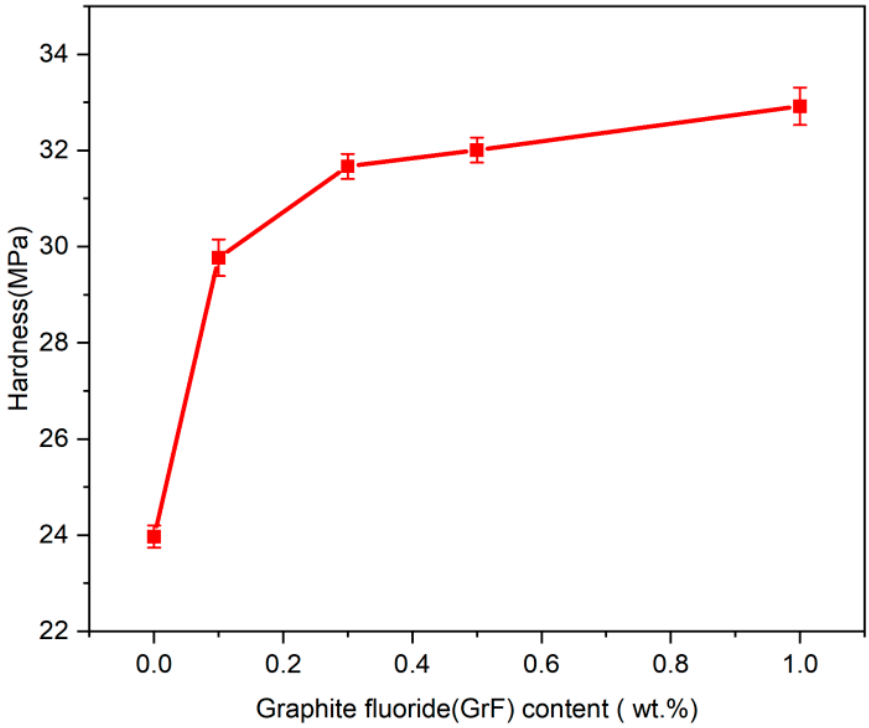

Figure 8. The hardness of the composites.

The hardness results of GrF-UHMW-PE composites showed a similar trend to those of the GO-UHMW-PE [45] and graphite-UHMW-PE [46] composites. According to the findings of Chen et al., [45] the addition of 1.0 wt.% GO resulted in an approximately 15% increase in the hardness of UHMW-PE. Similarly, Lorenzo-Bonet et al. [46] reported that the addition of 1.0 wt.% graphite enhanced the hardness of UHMW-PE by approximately 35%. In general, carbon fillers including GO, graphite, and GrF, exhibited superior mechanical properties compared to pure UHMW-PE. The presence of these enhanced particles in the composites allowed them to bear partial loads and facilitate the transmission of loads within the UHMW-PE matrix. As a result, incorporating these enhanced particles significantly enhanced the mechanical properties of UHMW-PE. Furthermore, in the case of the GrF-UHMW-PE composites, the presence of hydrogen bonds enhanced interface interactions that restricted the molecular-chain mobility of UHMW-PE around GrF platelets. This interaction was beneficial for transmitting stress from the UHMW-PE matrix to GrF, thereby enhancing the mechanical performance of the UHMW-PE matrix.

3.5. Tribological Properties of the Composites

3.5.1. The Coefficient of Friction (COF)

The addition of GrF had a significant impact on the COF of UHMW-PE, as depicted in Figure 9. Figure 9 illustrates the variation curve of the COF curve as a function of time and the

average COF values at different filler contents. Three samples with filler contents lower than 0.5 wt% initially experienced a rapid decrease in COF for a brief period, followed by a gradual increase. After a running-in period, the COF curve stabilized. However, when 1.0 wt% GrF was added, the COF initially increased for 1100 s and then remained stable. Additionally, it was observed that the curves for pure UHMW-PE, 0.1 wt% GrF-UHMW-PE, and 0.5 wt% GrF-UHMW-PE were relatively flatter compared to the curve of 1.0 wt% GrF-UHMW-PE.

The average COF of pure UHMW-PE was approximately 0.1020. The addition of a small amount of GrF (<0.5 wt%) led to a significant reduction in the COF of UHMW-PE. Notably, when 0.5 wt% of GrF was added, the lowest COF of 0.0666 was achieved. This represented a 34.76% decrease compared to pure UHMW-PE. However, further increasing the content of GrF to 1.0 wt% resulted in a significant increase in the COF, raising it from 0.0666 to 0.1402. This corresponded to a 37.31% increase compared to pure UHMW-PE.

It was well-known that UHMW-PE has a lower COF due to its self-lubricating properties [47]. Although carbon fillers including graphite, graphene, GO, and CNTs, have been shown to have excellent lubricating performances, their impact on the lubricity of UHMW-PE was generally limited and might have a negative effect in some circumstances. For example, when layered graphite [46] (0.1 wt%) was added to UHMW-PE, only a 13% reduction in COF was observed. However, based on the results of the above experiment, the addition of 0.5 wt% GrF resulted in a reduction of the COF of UHMW-PE to 35%. GrF, as an excellent solid lubricant, can reduce COF even in small amounts. The reason can be attributed to the characteristic structure of GrF. The fluoride atom bonded to the carbon atom in GrF resulted in an interlayer spacing of (001) planes of 6.88 Å (the above experimental results), which was larger than the d-spacing of graphite (3.40 Å) [48]. As a result, the expansion of the carbon layer planes facilitates sliding between the carbon layers under reciprocal frictional forces. In addition, during the friction process, GrF on the worn surface of the GrF-UHMW-PE composites was exposed and released, acting as a solid lubricant to reduce COF. The transfer films formed on the surface of the Si_2N_3 counterpart ball can also help reduce COF. On the contrary, a high filler content (1.0 wt%) in UHMW-PE could produce larger aggregated particles and increased surface roughness during the wear process (see SEM of worn surfaces), resulting in a higher COF than pure UHMW-PE.

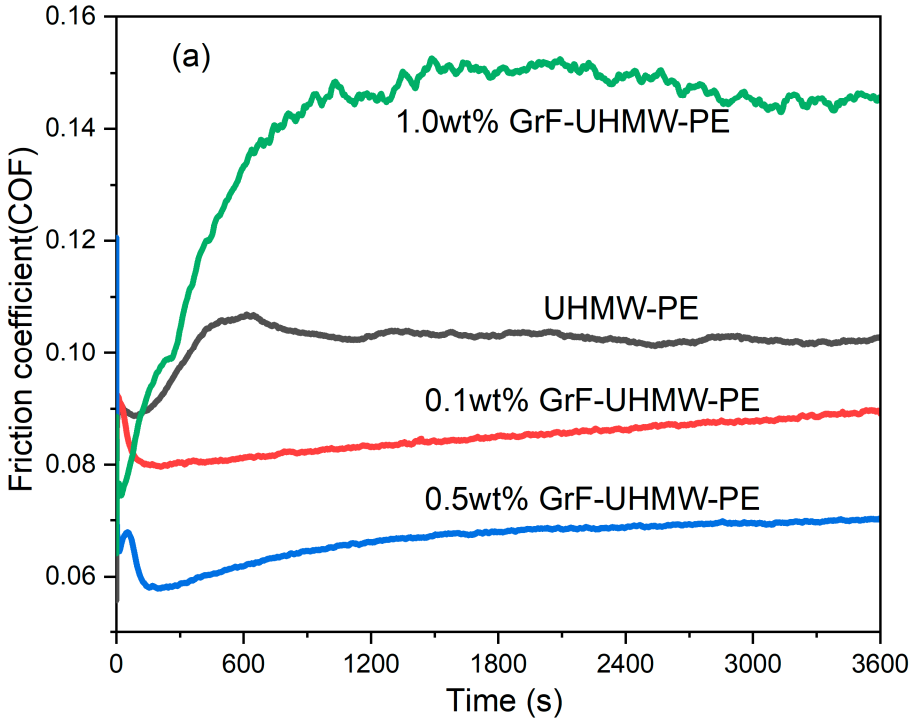

Figure 9. *Cont.*

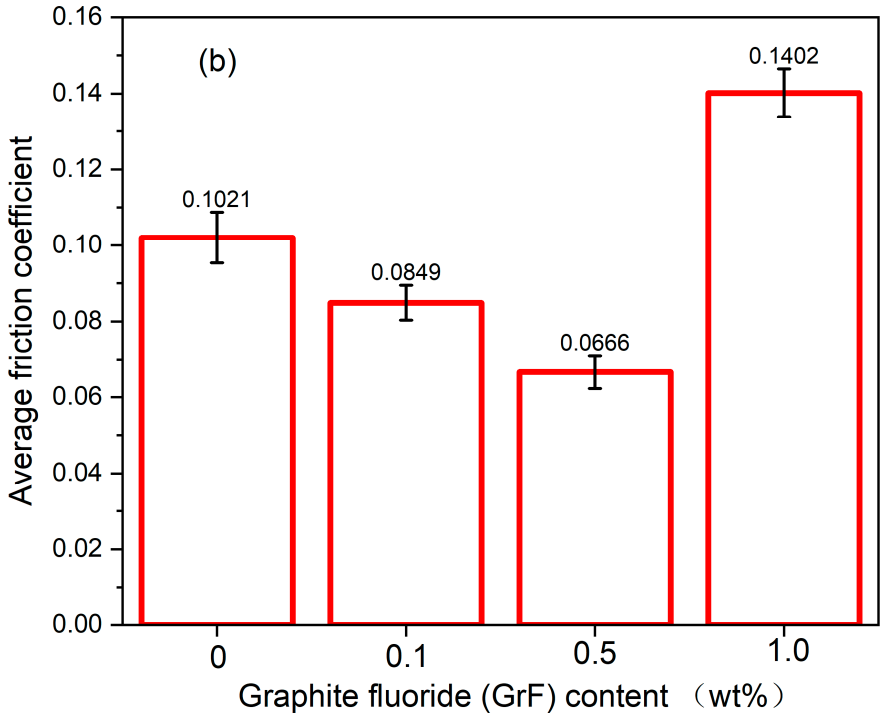

Figure 9. (**a**) Variation in COF with time, and (**b**) average COF.

3.5.2. The Wear of the Composites

In the reciprocating sliding tests, wear scars were produced by the Si_3N_4 counterparts. Figure 10 depicted the wear scars' three-dimensional and two-dimensional topography. The influence of the addition of GrF on the depth of wear scars can be observed in Figure 10. Adding 0.1 wt% GrF can significantly reduce the depth of wear. The further addition of GrF resulted in a further reduction in the depth of the wear scars, and the depth became the shallowest when the addition reached 0.5 wt%. However, when the addition amount was 1.0 wt% GrF, the depth of the composites was deeper than that of the composites with 0.5 wt% GrF.

Figure 11 depicts the composites' wear rates based on the results of Equation (8). The wear rates were determined by the amount of GrF. The wear rate of pure UHMW-PE was measured to be 8.13×10^{-5} mm^3 N^{-1} m^{-1}. With the addition of 0.1 wt% GrF in the UHMW-PE matrix, the wear rate decreased by 16.48%. Increasing the addition to 0.5 wt% GrF resulted in the wear rate reaching a minimum value of 4.25×10^{-5} mm^3 N^{-1} m^{-1}, reducing it by 47.72% compared to pure UHMW-PE. In contrast, raising the GrF content form 0.5 wt% to 1.0 wt% increased the wear rate. However, the wear rate was still lower in comparison to that of UHMW-PE.

These results of wear rates demonstrated that a lower addition of GrF had the potential to enhance the anti-wear performance of UHMW-PE. This enhancement can be attributed to the exceptional lubricant properties and mechanical characteristics of GrF. By acting as a solid lubricant, GrF effectively decreased the COF of UHMW-PE, resulting in a significant reduction in wear rate. Furthermore, the addition of GrF improved the hardness of the composites, thereby enhancing their tribological properties. In general, the wear resistance of the composites strongly influenced by their hardness [49]. Therefore, increasing the hardness further improved their anti-wear resistance. However, it is important to note that the high addition of GrF (1.0 wt%) led to accelerated wear, which can be attributed to its aggregation. The addition of 1.0 wt% GrF caused the formation of larger aggregated particles, leading to a high COF. This effect was stronger than that of solider lubrication.

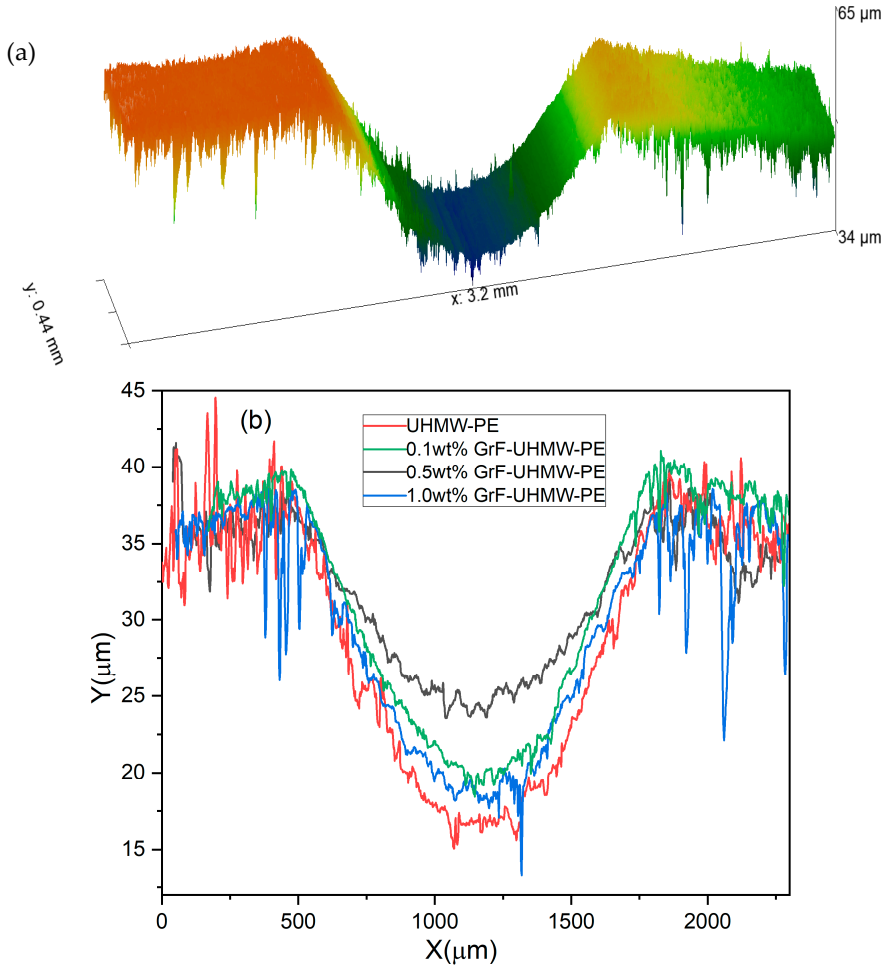

Figure 10. Wear profiles of the composites: (**a**) 3D profile of wear track, (**b**) 2D profile of wear track.

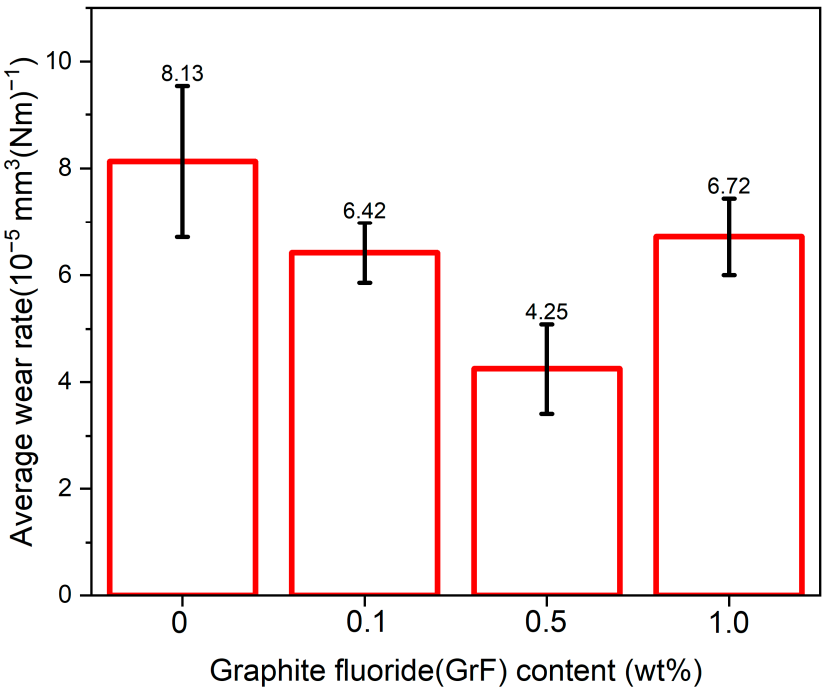

Figure 11. Wear rates of the composites.

3.5.3. SEM of Worn Surfaces and Wear Mechanism of the Composites

In order to investigate the wear mechanism of the composites, Figure 12 displays SEM images of the worn surface morphology of pure UHMW-PE and its composites with various GrF contents. As can be easily observed, the worn surface of pure UHMW-PE (Figure 12a) exhibited a number of cracks and delamination, which indicates that fatigue wear was the dominant mechanism for UHMW-PE. However, the incorporation of 0.1 wt% GrF into the UHMW-PE matrix significantly improved the worn surface. No visible cracks or delamination were found (Figure 12b), while some deeper scratches and extensive small pitting appeared, which suggests that the main wear mechanisms for this composite were fatigue wear and abrasive wear. As the GrF content increased to 0.5 wt%, the worn surface became relatively smooth (Figure 12c). As a result, it had a lower COF, which was consistent with the experimental results. Some pitting was also observed on the worn surface. Fatigue wear remained the predominant wear mechanism. Further increasing the GrF content to 1.0 wt% resulted in a significant deterioration of the worn surface (Figure 12d). Deeper abrasive grooves and larger wear debris particles characterized the severe wear scar surface, leading to increased surface roughness. Consequently, the COF also increased, which was consistent with the experimental results. The primary wear mechanism observed under these conditions was abrasive wear.

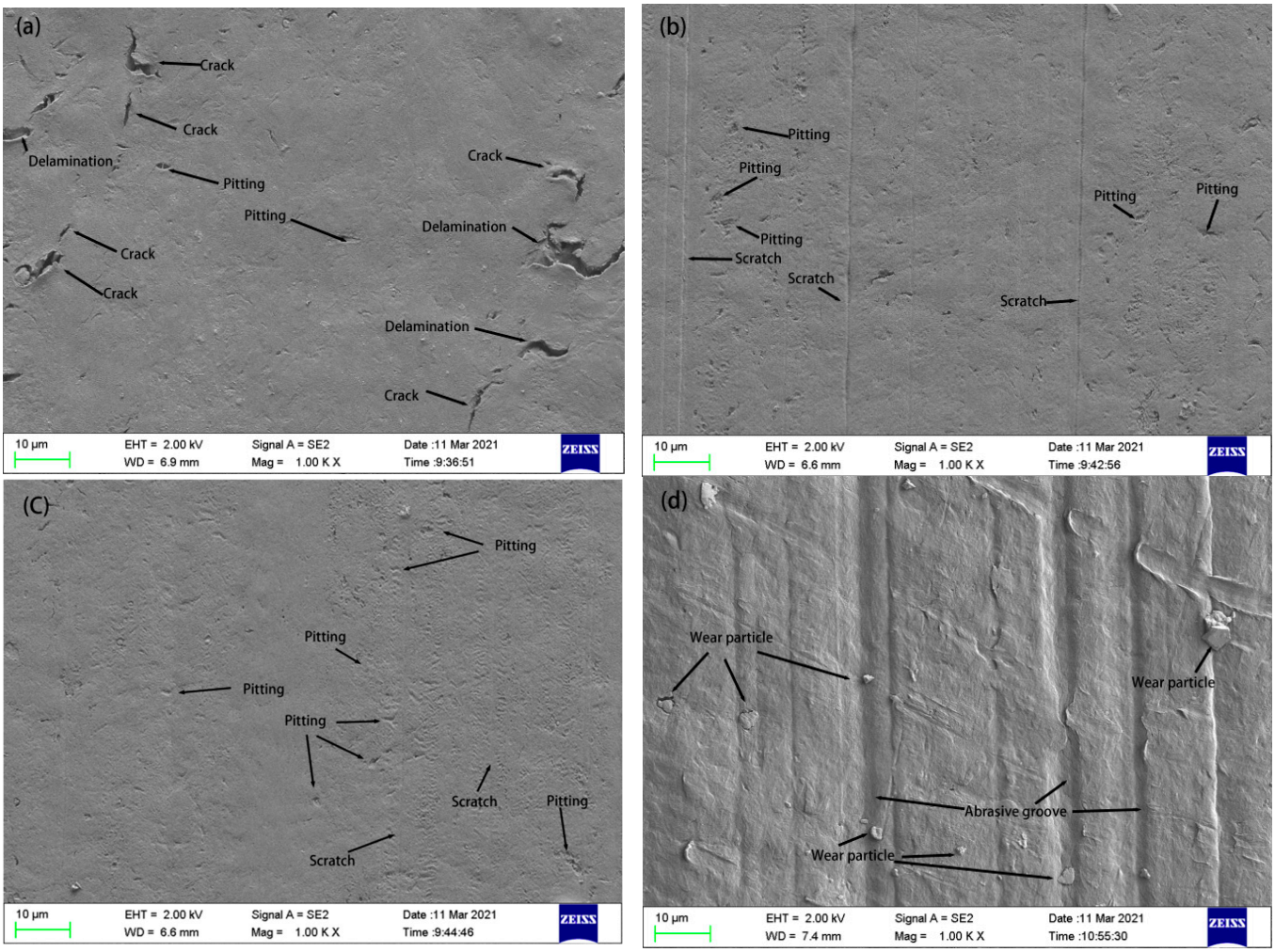

Figure 12. (**a**) Pure UHMW-PE, (**b**) filled 0.1 wt% GrF, (**c**) filled 0.5 wt% GrF, and (**d**) filled 1.0 wt% GrF.

In general, the main wear mechanism in polymer composites was abrasive wear [50] and fatigue wear [51]. These types of wear were characterized by the presence of cracks, scratches, furrows, and plastic deformation along the worn surface, which were caused

by point contact loads. During the friction between the polymer and Si_2O_3 ceramic ball, heat generation occurred, and as a result, thermal softening took place along the friction surface, which led to plastic deformation, scratches, and furrows on the wear surface. Figure 13 displayed a diagrammatic representation of the wear mechanisms. For the pure UHMW-PE friction process, the transfer membranes were formed on a ceramic ball and the friction process belonged to homogeneous material interaction. Fatigue cracks and delamination occurred under reciprocal cyclic stress due to the low mechanical properties of pure UHMW-PE. However, once heterogeneous GrF (0.1 wt%) was added and the mechanical properties of UHMW-PE were enhanced, abrasive scratches occurred because tougher wear particles, transfer films, and samples formed a three-body wear that was more likely to form scratches under cyclic stress. As the cycling process continued, micro-cracks were generated and propagated deeply into the polymer matrix, until one crack became large enough to break from the polymer, resulting in the occurrence of pitting. The addition of 0.5 wt% GrF to UHMW-PE matrix resulted in improved mechanical properties that effectively mitigated the detrimental effects of fatigue wear and abrasive wear, which led to a significant reduction in the occurrence of scratches and pitting. As a result, the worn surface was improved and exhibited a smoother surface. However, with the addition of GrF at higher concentrations, much larger wear particles were easily generated during the friction process due to the aggregation, which exacerbated three-body abrasion wear. Consequently, deeper abrasive grooves developed and caused an increase in the COF.

According to the above results, it can be concluded that the composites containing a lower content of GrF could efficiently enhance anti-wear properties and demonstrate resistance against fatigue-induced wear. The wear mechanisms were strongly dependent on GrF content. With the addition of GrF, the wear mechanism of the composites transformed from fatigue wear to abrasive wear.

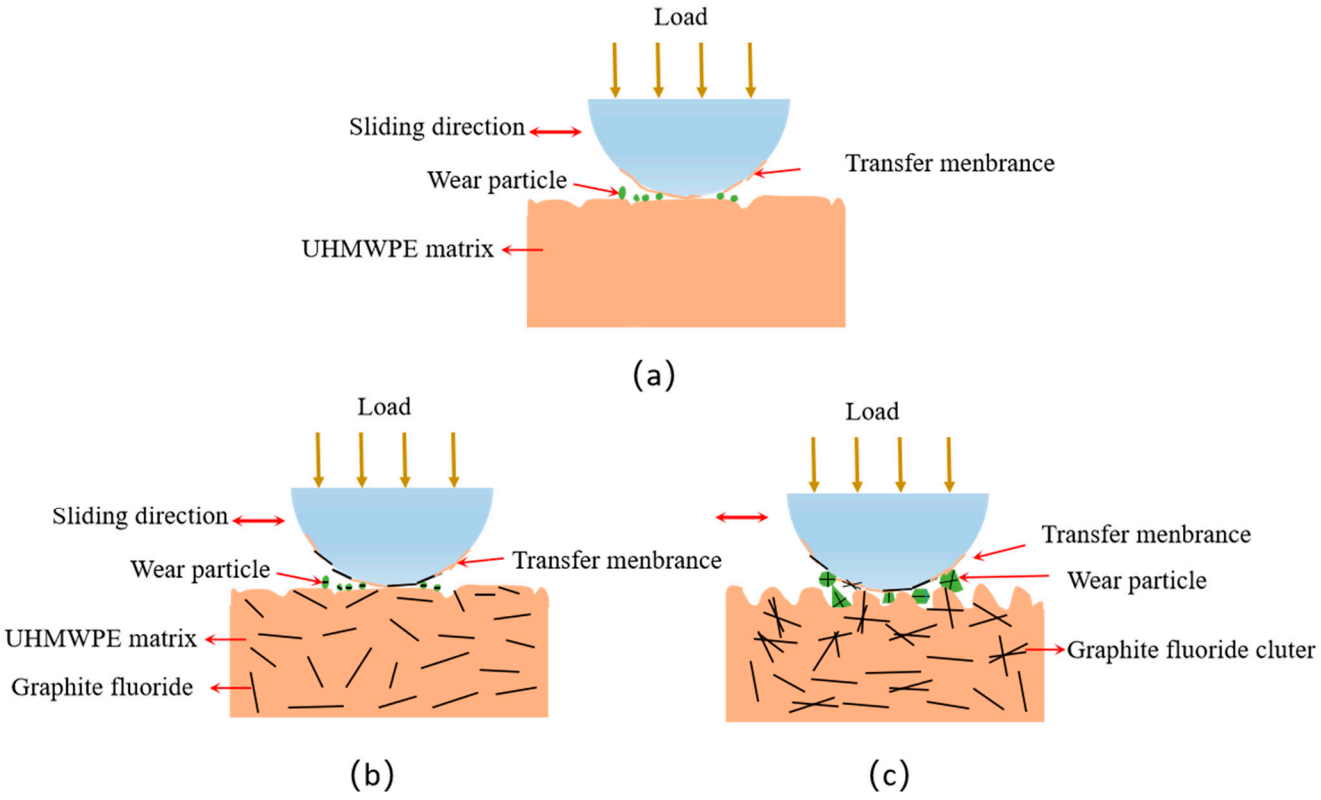

Figure 13. Schematic illustration of the wear mechanisms. (**a**) No addition, (**b**) lower addition (<=0.5 wt%), and (**c**) higher addition (1.0 wt%).

4. Conclusions

GrF, a novel solid lubricant, was incorporated into UHMW-PE and the GrF-UHMW-PE composites were successfully prepared. The structure, hardness, and tribological properties of the composites were investigated. The results were as follows:

1. The hydrogen bonds (C-F···H-C) were formed and enhanced interfacial interaction between GrF and UHMW-PE, according to the results of FT-IR spectrometry.
2. Adding GrF can significantly enhance the hardness of the composites. At 1.0 wt% GrF, the hardness increased by 37%, compared to pure UHMW-PE.
3. At a lower GrF concentration, GrF exhibited remarkable lubricant properties and anti-wear properties. At 0.5 wt% GrF concentration, the COF and wear rate were reduced by 34.76% and 47.72%, respectively, compared to the UHMW-PE. At a high GrF concentration, the COF significantly increased while the anti-wear properties decreased.
4. As the concentration of GrF increased, the wear modes of the composites transitioned from fatigue wear to abrasive wear.

Author Contributions: Conceptualization, G.H. and Y.C.; methodology, G.H.; software, H.H.; validation, G.H., F.Y. and Y.Z.; formal analysis, G.H.; investigation, G.H.; resources, G.H.; data curation, F.Y.; writing—original draft preparation, G.H.; writing—review and editing, G.H.; visualization, H.H.; supervision, Y.Z.; project administration, T.Z.; funding acquisition, T.Z. All authors have read and agreed to the published version of the manuscript.

Funding: This research was funded by the Jiangsu Natural Science Foundation (No. BK20201142), Top-notch Academic Programs Project of Jiangsu Higher Education Institutions (Grant no. PPZY2015B186), Suzhou Key Laboratory Support Project (Grant no. SZS201815) and the National Natural Science Foundation of China (Grant no. 51675232).

Data Availability Statement: Not applicable.

Conflicts of Interest: The authors declare no conflict of interest.

References

1. Kurtz, S.M. *UHMWPE Biomaterials Handbook: Ultra High Molecular Weight Polyethylene in Total Joint Replacement and Medical Devices*; Academic Press: Cambridge, MA, USA, 2009.
2. Anaya-Garza, K.; Domínguez-Crespo, M.; Torres-Huerta, A.; Brachetti-Sibaja, S.; Moreno-Palmerin, J. UHMWPE/OPA Composite Coatings on Ti6Al4V Alloy as Protective Barriers in a Biological-Like Medium. In *Environmental Concerns and Remediation: Proceedings of F-EIR Conference 2021*; Springer: Cham, Switzerland, 2022; pp. 1–12.
3. Liu, Z.; Du, Y.; Ma, H.; Li, J.; Zhang, X.; Zhu, E.; Shi, C.; Zhu, Z.; Zhao, S. Mechanism of boron carbide particles improving the wear resistance of UHMWPE: Structure-property relationship. *Polymer* **2022**, *245*, 124733. [CrossRef]
4. Rahman, M.M.; Biswas, M.A.S.; Hoque, K.N. Recent development on micro-texturing of UHMWPE surfaces for orthopedic bearings: A review. *Biotribology* **2022**, *31*, 100216. [CrossRef]
5. Patil, N.A.; Njuguna, J.; Kandasubramanian, B. UHMWPE for biomedical applications: Performance and functionalization. *Eur. Polym. J.* **2020**, *125*, 109529. [CrossRef]
6. Bistolfi, A.; Giustra, F.; Bosco, F.; Sabatini, L.; Aprato, A.; Bracco, P.; Bellare, A. Ultra-high molecular weight polyethylene (UHMWPE) for hip and knee arthroplasty: The present and the future. *J. Orthop.* **2021**, *25*, 98–106. [CrossRef]
7. Baena, J.C.; Wu, J.; Peng, Z. Wear performance of UHMWPE and reinforced UHMWPE composites in arthroplasty applications: A review. *Lubricants* **2015**, *3*, 413–436. [CrossRef]
8. Kandahari, A.M.; Yang, X.; Laroche, K.A.; Dighe, A.S.; Pan, D.; Cui, Q. A review of UHMWPE wear-induced osteolysis: The role for early detection of the immune response. *Bone Res.* **2016**, *4*, 16014. [CrossRef]
9. Dwivedi, Y.; Laurent, M.P.; Sarvepalli, S.; Schmid, T.M.; Wimmer, M.A. Albumin protein cleavage affects the wear and friction of ultra-high molecular weight polyethylene. *Lubricants* **2017**, *5*, 33. [CrossRef]
10. Dangsheng, X. Friction and wear properties of UHMWPE composites reinforced with carbon fiber. *Mater. Lett.* **2005**, *59*, 175–179. [CrossRef]
11. Wang, L.L.; Zhang, L.Q.; Tian, M. Mechanical and tribological properties of acrylonitrile–butadiene rubber filled with graphite and carbon black. *Mater. Des.* **2012**, *39*, 450–457. [CrossRef]
12. Moghadam, A.D.; Omrani, E.; Menezes, P.L.; Rohatgi, P.K. Mechanical and tribological properties of self-lubricating metal matrix nanocomposites reinforced by carbon nanotubes (CNTs) and graphene—A review. *Compos. Part B Eng.* **2015**, *77*, 402–420. [CrossRef]

13. Khun, N.W.; Zhang, H.; Lim, L.H.; Yang, J. Mechanical and tribological properties of graphene modified epoxy composites. *Appl. Sci. Eng. Prog.* **2015**, *8*, 101–109.
14. Miao, X.; Li, Z.; Liu, S.; Hou, K.; Wang, J.; Yang, S. Ionic bridging strengthened MXene/GO nanocomposite films with extraordinary mechanical and tribological properties. *Appl. Surf. Sci.* **2023**, *625*, 157181. [CrossRef]
15. Huang, Z.; Zheng, Z.; Zhao, S.; Dong, S.; Luo, P.; Chen, L. Copper matrix composites reinforced by aligned carbon nanotubes: Mechanical and tribological properties. *Mater. Des.* **2017**, *133*, 570–578. [CrossRef]
16. Zhou, S.; Zhang, Q.; Wu, C.; Huang, J. Effect of carbon fiber reinforcement on the mechanical and tribological properties of polyamide6/polyphenylene sulfide composites. *Mater. Des.* **2013**, *44*, 493–499. [CrossRef]
17. Pang, W.; Wu, J.; Zhang, Q.; Li, G. Graphene oxide enhanced, radiation cross-linked, vitamin E stabilized oxidation resistant UHMWPE with high hardness and tensile properties. *RSC Adv.* **2017**, *7*, 55536–55546. [CrossRef]
18. Ni, Z.; Pang, W.; Chen, G.; Lu, P.; Qian, S. The influence of irradiation on thermal and mechanical properties of UHMWPE/GO nanocomposites. *Russ. J. Appl. Chem.* **2017**, *90*, 1876–1882. [CrossRef]
19. Tai, Z.; Chen, Y.; An, Y.; Yan, X.; Xue, Q. Tribological behavior of UHMWPE reinforced with graphene oxide nanosheets. *Tribol. Lett.* **2012**, *46*, 55–63. [CrossRef]
20. Bhattacharyya, A.; Chen, S.; Zhu, M. Graphene reinforced ultra high molecular weight polyethylene with improved tensile strength and creep resistance properties. *Express Polym. Lett.* **2014**, *8*, 74–84. [CrossRef]
21. Chih, A.; Ansón-Casaos, A.; Puértolas, J. Frictional and mechanical behaviour of graphene/UHMWPE composite coatings. *Tribol. Int.* **2017**, *116*, 295–302. [CrossRef]
22. Reddy, K.S.N.; Unnikrishnan, D.; Balachandran, M. Investigation and optimization of mechanical, thermal and tribological properties of UHMWPE–graphite nanocomposites. *Mater. Today Proc.* **2018**, *5*, 25139–25148. [CrossRef]
23. Di Vittorio, S.; Dresselhaus, M.; Dresselhaus, G. A model for disorder in fluorine-intercalated graphite. *J. Mater. Res.* **1993**, *8*, 1578–1585. [CrossRef]
24. Yang, L.; Li, Y.; Wang, L.; Pei, Y.; Wang, Z.; Zhang, Y.; Lin, H.; Li, X. Exfoliated fluorographene quantum dots as outstanding passivants for improved flexible perovskite solar cells. *ACS Appl. Mater. Interfaces* **2020**, *12*, 22992–23001. [CrossRef] [PubMed]
25. Giraudet, J.; Claves, D.; Guérin, K.; Dubois, M.; Houdayer, A.; Masin, F.; Hamwi, A. Magnesium batteries: Towards a first use of graphite fluorides. *J. Power Sources* **2007**, *173*, 592–598. [CrossRef]
26. Kumaran, A.A.; Chithrambattu, A.; Vedhanarayanan, B.; Rajukrishnan, S.B.A.; Praveen, V.K.; Kizhakayil, R.N. Fluoride-philic reduced graphene oxide–fluorophore anion sensors. *Mater. Adv.* **2022**, *3*, 6809–6817. [CrossRef]
27. Zhao, F.-G.; Kong, Y.-T.; Pan, B.; Hu, C.-M.; Zuo, B.; Dong, X.; Li, B.; Li, W.-S. In situ tunable pillaring of compact and high-density graphite fluoride with pseudocapacitive diamines for supercapacitors with combined predominance in gravimetric and volumetric performances. *J. Mater. Chem. A* **2019**, *7*, 3353–3365. [CrossRef]
28. Lei, F.; Wu, B.; Sun, H.; Jiang, F.; Yang, J.; Sun, D. Simultaneously improving the anticorrosion and antiscratch performance of epoxy coatings with graphite fluoride via large-scale preparation. *Ind. Eng. Chem. Res.* **2018**, *57*, 16709–16717. [CrossRef]
29. Mittal, D.; Singh, D.; Sharma, S.K. Thermal characteristics and tribological performances of solid lubricants: A mini review. *Adv. Rheol. Mater.* **2023**. [CrossRef]
30. Fusaro, R.L.; Sliney, H.E. Graphite fluoride (CFx) n—A new solid lubricant. *Asle Trans.* **1970**, *13*, 56–65. [CrossRef]
31. Thomas, P.; Bilas, P.; Molza, A.; Legras, L.; Mansot, J.L.; Guérin, K.; Dubois, M. 14—Fluorinated Nanocarbons for Lubrication. In *New Fluorinated Carbons: Fundamentals and Applications*; Boltalina, O.V., Nakajima, T., Eds.; Elsevier: Boston, MA, USA, 2017; pp. 325–360.
32. Fusaro, R.L.; Sliney, H.E. *Preliminary Investigation of Graphite Fluoride (CF X) N as a Solid Lubricant*; National Aeronautics and Space Administration: Washington, DC, USA, 1969.
33. Fusaro, R.L.; Sliney, H.E. Lubricating characteristics of polyimide bonded graphite fluoride and polyimide thin films. *ASLE Trans.* **1973**, *16*, 189–196. [CrossRef]
34. Yan, Y.T.; Wang, R.; Song, W.L. The preparation and Tribological Properties of graphite fluoride. *Adv. Mater. Res.* **2014**, *941*, 1544–1547. [CrossRef]
35. Sun, H.; Jiang, F.; Lei, F.; Chen, L.; Zhang, H.; Leng, J.; Sun, D. Graphite fluoride reinforced PA6 composites: Crystallization and mechanical properties. *Mater. Today Commun.* **2018**, *16*, 217–225. [CrossRef]
36. Sun, H.; Li, T.; Lei, F.; Yang, M.; Li, D.; Huang, X.; Sun, D. Graphite fluoride and fluorographene as a new class of solid lubricant additives for high-performance polyamide 66 composites with excellent mechanical and tribological properties. *Polym. Int.* **2020**, *69*, 457–466. [CrossRef]
37. Lu, P.; Wu, M.; Ni, Z.; Huang, G. Oxidative degradation behavior of irradiated GO/UHMWPE nanocomposites immersed in simulated body fluid. *Polym. Bull.* **2021**, *78*, 5153–5164. [CrossRef]
38. Hertz, H. The contact of elastic solids. *J. Reine. Angew. Math.* **1881**, *92*, 156–171.
39. Zdero, R.; Bagheri, Z.S.; Rezaey, M.; Schemitsch, E.H.; Bougherara, H. The biomechanical effect of loading speed on Metal-on-UHMWPE contact mechanics. *Open Biomed. Eng. J.* **2014**, *8*, 28. [CrossRef]
40. Kapps, V.; Maru, M.M.; Kuznetsov, O.; Achete, C.A. Identifying differences in the tribological performance of GUR 1020 and GUR 1050 UHMWPE resins associated to pressure× velocity conditions in linear reciprocating sliding tests. *J. Mech. Behav. Biomed. Mater.* **2023**, *145*, 106038. [CrossRef] [PubMed]

41. Pang, W.; Ni, Z.; Chen, G.; Huang, G.; Huang, H.; Zhao, Y. Mechanical and thermal properties of graphene oxide/ultrahigh molecular weight polyethylene nanocomposites. *Rsc Adv.* **2015**, *5*, 63063–63072. [CrossRef]
42. Shafiee, M.; Aamazani SA, A. Optimization of UHMWPE/graphene nanocomposite processing using ziegler-natta catalytic system via response surface methodology. *Polym.-Plast. Technol. Eng.* **2014**, *53*, 969–974. [CrossRef]
43. Zhao, Y.; Wang, M.; Tang, Z.; Wu, G. Radiation effects of UHMW-PE fibre on gel fraction and mechanical properties. *Radiat. Phys. Chem.* **2011**, *80*, 274–277. [CrossRef]
44. Thalladi, V.R.; Weiss, H.-C.; Bläser, D.; Boese, R.; Nangia, A.; Desiraju, G.R. C−H···F Interactions in the Crystal Structures of Some Fluorobenzenes. *J. Am. Chem. Soc.* **1998**, *120*, 8702–8710. [CrossRef]
45. Chen, Y.; Qi, Y.; Tai, Z.; Yan, X.; Zhu, F.; Xue, Q. Preparation, mechanical properties and biocompatibility of graphene oxide/ultrahigh molecular weight polyethylene composites. *Eur. Polym. J.* **2012**, *48*, 1026–1033. [CrossRef]
46. Lorenzo-Bonet, E.; Hernandez-Rodriguez, M.A.L.; Perez-Acosta, O.; De la Garza-Ramos, M.A.; Contreras-Hernandez, G.; Juarez-Hernandez, A. Characterization and tribological analysis of graphite/ultra high molecular weight polyethylene nanocomposite films. *Wear* **2019**, *426–427*, 195–203. [CrossRef]
47. Aliyu, I.K.; Mohammed, A.S.; Al-Qutub, A. Tribological Performance of UHMWPE/GNPs Nanocomposite Coatings for Solid Lubrication in Bearing Applications. *Tribol. Lett.* **2018**, *66*, 144. [CrossRef]
48. Tsai, J.-L.; Tu, J.-F. Characterizing mechanical properties of graphite using molecular dynamics simulation. *Mater. Des.* **2010**, *31*, 194–199. [CrossRef]
49. Momber, A.W.; Irmer, M.; Marquardt, T. Effects of polymer hardness on the abrasive wear resistance of thick organic offshore coatings. *Prog. Org. Coat.* **2020**, *146*, 105720. [CrossRef]
50. Unal, H.; Sen, U.; Mimaroglu, A. Abrasive wear behaviour of polymeric materials. *Mater. Des.* **2005**, *26*, 705–710. [CrossRef]
51. Zhao, G.; Wang, T.; Wang, Q. Friction and wear behavior of the polyurethane composites reinforced with potassium titanate whiskers under dry sliding and water lubrication. *J. Mater. Sci.* **2011**, *46*, 6673–6681. [CrossRef]